Inorganic Chemistry

Article

pubs.acs.org/IC

From Uranothorites to Coffinite: A Solid Solution Route to the Thermodynamic Properties of $USiO_4$

Stéphanie Szenknect,*[,†] Dan T. Costin,[†] Nicolas Clavier,[†] Adel Mesbah,[†] Christophe Poinssot,[‡] Pierre Vitorge,[§] and Nicolas Dacheux[†]

[†]ICSM, UMR 5257 CEA/CNRS/UM2/ENSCM, Site de Marcoule − Bât. 426, BP 17171, 30207 Bagnols-sur-Cèze cedex, France

[‡]CEA, Nuclear Energy Division, DRCP/DIR, CEA Marcoule, Bât. 400, BP 17171, 30207 Bagnols-sur-Cèze cedex, France

[§]CEA, Nuclear Energy Division, DPC/SECR, Site de Saclay, Bât. 391, 91191 Gif-sur-Yvette, France

Supporting Information

ABSTRACT: Experiments on the solubility of intermediate members of the $Th_{1-x}U_xSiO_4$ solid solution were carried out to determine the impact of Th−U substitutions on the thermodynamic properties of the solid solution and then allow extrapolation to the coffinite end member. The ion activity products in solutions equilibrated with $Th_{1-x}U_xSiO_4$ ($0 \le x \le 0.5$) were determined by dissolution experiments conducted in 0.1 mol·L^{-1} HCl under Ar atmosphere at several temperatures ranging from 298 to 346 K. For all experiments, dissolution was congruent, and a constant composition of the aqueous solution was reached after 50−200 days of dissolution. The solubility product of thorite was determined (log $^*K_{S,ThSiO_4} = -5.62 \pm 0.08$) whereas the solubility product of coffinite was estimated (log $^*K_{S,USiO_4} = -6.1 \pm 0.2$). The stoichiometric solubility product of $Th_{1-x}U_xSiO_4$ reached a maximum value for $x = 0.45 \pm 0.05$. In terms of the standard Gibbs free energy of dissolution, solid solutions dissolve more spontaneously than the end members. The standard Gibbs free energy associated with the formation of thorite, coffinite, and intermediate members of the series were then evaluated. The standard Gibbs free energies of formation were found to increase linearly with the uranium mole fraction. Our data at low temperature clearly show that uranothorite solid solutions with $x > 0.26$, thus coffinite, are less stable than the mixture of binary oxides, which is consistent with qualitative evidence from petrographic studies of uranium ore deposits.

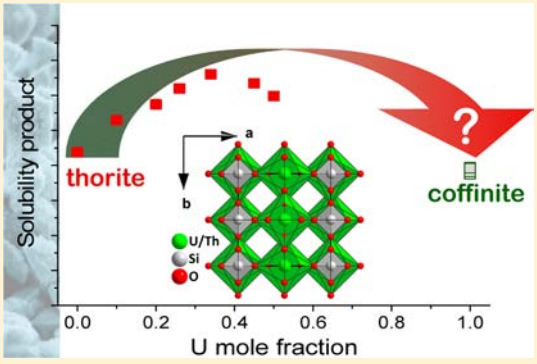

1. INTRODUCTION

Coffinite, $USiO_4$, is one of the major U(IV) minerals in economically exploitable reduced uranium ore deposits, often associated with pitchblende.[1] Given the ubiquity of dissolved silica, coffinite is the second most abundant source of uranium in the geosphere.[2] In addition, the direct disposal of spent nuclear fuel (SNF) in deep geologic formations is considered as a waste management option in several countries.[3,4] Conservative safety assessments consider that the SNF comes into contact with groundwater after the long-term degradation of confinement barriers. Secondary phases that could be formed during radwaste leaching represent important sinks for uranium and other radionuclides and thus control the subsequent mobility and the ultimate distribution of the radiotoxic elements in the surrounding environment. Most of the sites under investigation for an underground repository are located in undisturbed claystone exhibiting anoxic conditions and a silica-enriched environment.[5] Such geochemical conditions impose circumneutral pH and low redox potential ($Eh_{SHE} \approx -200$ mV) that favor the formation of U(IV) secondary phases after the dissolution of the UO_2 matrix.[6] In addition, the estimated concentration of Si in such claystone pore water[7] exceeds 10^{-4} mol·L^{-1}. Under these conditions, coffinite is suspected to precipitate and then to impact the uranium release based on the relative stability of coffinite and uraninite.[6] Indeed, coffinite was identified as an alteration product of uraninite UO_{2+x} in U deposits considered as SNF repository analogs[8] at Oklo, Gabon, Palamottu, Finland,[9] and Cigar Lake, Canada.[10,11]

However, the thermodynamic properties associated with coffinite, especially the solubility product constant, remain poorly defined. Very few reliable thermodynamic data related to coffinite formation or solubility are reported in the literature. These data were estimated from qualitative experiments and available geological information. The variation of the standard Gibbs free energy related to the formation of $USiO_4$ validated by the NEA Thermodynamic DataBase (NEA TDB) project[12,13] was estimated at -1883.6 ± 4.0 kJ·mol^{-1} at 298.15 K. This value was based on the Langmuir assumption.[14] It mainly implies that the average silica concentration (about 10^{-3} mol·L^{-1}) found in groundwater draining the Grants Mineral Belt in New Mexico (USA), where both uraninite and coffinite occur in ore deposits, represents a good estimate of the equilibrium silica activity for reaction 1:

$$USiO_4(s) + 2H_2O \leftrightarrows UO_2(s) + H_4SiO_4(aq) \quad (1)$$

Received: February 1, 2013
Published: May 30, 2013

The thermal stability of coffinite is also not well-known. Fuchs and Hoekstra[15] placed the upper limit of coffinite stability compared with uraninite and amorphous silica at 1273 K. On the basis of this observation, Hemingway[16] estimated the variation of the Gibbs free energy related to the formation of coffinite at 298.15 K assuming that the $\Delta_R G^\circ$ value associated with reaction 2 is equal to zero at 1273 K and using the heat capacities of quartz and uraninite to estimate the heat capacity of coffinite between 298.15 and 1273 K:

$$UO_2(s) + SiO_2(s) \leftrightarrows USiO_4(s) \quad (2)$$

The value obtained by Hemingway for $\Delta_f G^\circ$ was -1886 ± 6 kJ·mol^{-1}, which is compatible with the NEA TDB value. Thus, coffinite would be less stable than uraninite and quartz at 298.15 K. A value of -2028 kJ·mol^{-1} was also determined more recently by *ab initio* calculations.[17] None of these values were determined experimentally by solubility or thermochemical measurements.

Solubility or thermochemical studies require pure single-phase $USiO_4$. Most of the natural samples contain coffinite as very small grain crystals (~5 μm)[10] and in intimate intergrowths with large amounts of associated minerals. Moreover, for several decades persistent difficulties have been encountered in the preparation of pure single-phase synthetic coffinite. $USiO_4$ formation was clearly evidenced by precipitation under hydrothermal conditions, but UO_2 and amorphous SiO_2 were systematically observed as secondary phases.[15,18−21] Pointeau et al. (2009)[19] suggested that these difficulties might be related to the narrow Eh/pH range for thermodynamic stability of coffinite and by kinetic control of coffinite precipitation. The latter assumption was recently confirmed by Costin et al. (2011),[22] who showed that the mechanism of formation of $Th_{1-x}U_xSiO_4$ solid solutions through a dissolution/reprecipitation process under hydrothermal conditions slows with increasing U content. Thus the formation of coffinite, even if thermodynamically achievable, should be scarcely observable on a laboratory time scale.

Since the previous attempts failed to synthesize large amounts of pure single-phase coffinite for solubility studies, an indirect method based on solubility measurements of $Th_{1-x}U_xSiO_4$ samples was envisaged. Indeed, $ThSiO_4$ (thorite) and coffinite are isomorphic,[23−25] and the existence of uranothorite solid solutions has been clearly evidenced in granites.[26−28] The preparation of synthetic $Th_{1-x}U_xSiO_4$ uranothorite solid solutions was successfully undertaken under hydrothermal conditions (T = 250 °C) by Costin et al.[21,22] The formation of a complete solid solution series between x = 0 (thorite) and x = 0.8 was evidenced by PXRD and EDS analyses. A set of experiments on the solubility of intermediate members of the uranothorite solid solution series was thus carried out. The objective of this study was to determine the impact of uranium to thorium substitutions on the variability of the thermodynamic properties of the uranothorite solid solutions and then to allow their extrapolation to the coffinite end member.

2. EXPERIMENTAL SECTION

2.1. Synthesis Procedure. All $Th_{1-x}U_xSiO_4$ samples were prepared following the protocol detailed in Costin et al.[21,22] Briefly, all the reagents were of analytical grade and supplied by Sigma-Aldrich, except uranium chloride solutions prepared by dissolving uranium metal chips in a solution of 6 mol·L^{-1} HCl.[29] Also, the thorium chloride concentrated solution was obtained by dissolving thorium nitrate pentahydrate supplied by Sigma-Aldrich in a solution of 8 mol·L^{-1} HCl. Several cycles of evaporation and dissolution in a solution of 8 mol·L^{-1} HCl were undertaken until all traces of nitrates were eliminated.[30] The mass concentrations of the uranium chloride solution and thorium chloride solution used for the syntheses were determined by ICP-AES and were, respectively, 3.72×10^{-4} and 4.04×10^{-4} mol·g^{-1}. In order to prevent any oxidation of U(IV) to U(VI), the synthesis was performed in an inert glovebox flushed with Ar (with less than 1 ppm O_2). Stoichiometric amounts of thorium and uranium chloride were first mixed and diluted in 5 mL of deionized water to obtain 1 mmol of homogeneous starting solution with the desired x ratio ($0 \le x \le 0.8$), which was added dropwise to 5 mL of an aqueous solution containing 1.03 mmol of Na_2SiO_3. The pH was then raised close to 9 by adding 8 mol·L^{-1} NaOH and buffered to 8.6 ± 0.1 by adding $NaHCO_3$. The resulting gel was poured in a PTFE-lined Parr Instruments autoclave (V = 23 mL), then heated under hydrothermal conditions to 250 °C for 24 h, except for the solids with x = 0.4, 0.45, and 0.5, which were heated for longer times (48−64 h). The resulting precipitates were separated from the supernatant by centrifugation, washed three times with deionized water and ethanol, and then finally dried overnight at 60 °C.

2.2. Solid Characterizations. Scanning electron microscopy (SEM) analyses were conducted using an FEI Quanta 200 electron microscope equipped either with an Everhart−Thornley detector (ETD) or a backscattered electron detector (BSED) in high vacuum conditions with a very low accelerating voltage (2−3.1 kV). These conditions produced high-resolution images. Small powder samples were then directly analyzed without any preparation. X-ray energy-dispersive spectroscopy (EDS) analyses were performed using the Bruker AXS X-Flash 5010 detector coupled to the SEM device. To quantify atomic percentages, the powders were first embedded in epoxy resin. The surface of the samples was then polished to optical grade and metallized by carbon deposition. Experimental data were finally collected from 30 different locations using ThO_2, UO_2, and albite ($NaAlSi_3O_8$) as standards.

Powder X-ray diffraction (PXRD) patterns were recorded on a Bruker D8 Advance diffractometer equipped with a LynxEye detector in Bragg−Brentano geometry and using Cu K$\alpha_{1,2}$ radiation (λ = 1.5418 Å). PXRD patterns were recorded at room temperature in the $5° \le 2\theta \le 100°$ range with a step size of 0.01° and a total counting time of 4 h per sample. Pure silicon was measured under the same conditions and used as standard to extract the instrumental function. All powder patterns were refined thoroughly by the Rietveld method using the Thompson−Cox−Hastings pseudo-Voigt function convoluted with an axial divergence asymmetry function[31] with the FullProf Suite.[32] During the refinement, the following parameters were allowed to vary: zero shift, scale factors, preferred orientation (uranothorite, *I*4/*amd*), lattice parameters, and the overall thermal displacement for each phase. Furthermore, broadening effect was treated by considering an anisotropic size model. The chemical occupancy of the U/Th site was fixed to the values obtained by X-EDS.

Finally, specific surface area measurements were carried out using N_2 adsorption at 77 K and the BET method with a Micromeritics ASAP 2020 device.

2.3. Dissolution Experiments. The solids used for dissolution experiments were chosen based on their U loading. The main properties of the samples are listed in Table 1. The powders were purified before dissolution experiments in order to eliminate any impurities (mixed dioxides and silica) that remained from the synthesis protocol. Each purification cycle consisted of several steps: first, 200 mg of solid was contacted with 50 mL of 1 mol·L^{-1} HNO_3 for 16 h; second the solid was centrifuged and washed three times in deionized water; and third, the remaining solid was dispersed in 50 mL of 10^{-2} mol·L^{-1} KOH for 16 h, then washed three times with deionized water. Two purification cycles were performed and the samples were finally dried overnight in an oven at 60 °C. PXRD patterns were then recorded, EDS analyses were performed, and the (U+Th/Si) ratio of the samples was checked to ensure uranothorite composition.

All the dissolution experiments were performed under anoxic conditions controlled by flushing the glovebox with Ar. Purified samples (100 mg) were introduced into sealed polytetrafluoroethylene (PTFE) jars (Savillex) and contacted with 30 mL of 0.1 mol·L^{-1} HCl solution prepared under Ar bubbling. The low pH was chosen to increase the dissolution rate and shorten the dissolution time required to reach thermodynamic equilibrium. All the experiments at 298 ± 2 K were performed in duplicate. For experiments performed at higher temperatures (from 313 ± 2 to 346 ± 2 K), the dissolution vessels were placed

dx.doi.org/10.1021/ic400272s | Inorg. Chem. 2013, 52, 6957−6968

Table 1. X-EDS Analyses of the Samples Used for Solubility Experiments[a]

	X-EDS analyses				Rietveld refinements				N_2 adsorption
x (expected)	U (at. %)	Th (at. %)	An/Si	x_{exp} (EDS)	a (Å)	c (Å)	V_{cell} (Å^3)	x (PXRD)	A_{BET} (m^2 g^{-1})
0	0	17.1(2)	1.06(2)	**0**	7.148(1)	6.309(1)	322.8(7)	**0**	18
0.1	1.5(1)	15.0(2)	0.99(2)	**0.09(1)**	7.119(1)	6.317(1)	320.2(6)	**0.09(1)**	35
0.2	3.3(2)	13.0(3)	0.96(4)	**0.20(1)**	7.091(1)	6.312(1)	317.4(5)	**0.17(1)**	21
0.3	4.4(1)	12.3(2)	1.00(2)	**0.26(1)**	7.087(2)	6.315(2)	316.5(1)	**0.24(2)**	16
0.4	5.7(4)	11.0(3)	0.99(4)	**0.35(2)**	7.069(3)	6.305(1)	315.1(6)	**0.34(3)**	9
0.45	7.5(2)	8.9(2)	0.96(1)	**0.45(1)**	7.051(1)	6.303(1)	313.3(1)	**0.45(1)**	9
0.5	8.6(3)	8.2(3)	1.01(3)	**0.51(1)**	7.048(1)	6.294(1)	312.6(1)	**0.46(2)**	11

[a]The corresponding unit cell parameters of the uranothorite solid solutions were obtained by the Rietveld method, and the specific surface area was determined by N_2 adsorption and the BET method.

in thermostatic aluminum baths. The dissolution was carried out for almost 1 year at room temperature. During this time, the dissolution reactors were stirred at least twice a week. The dissolution of the solid was then monitored through regular pH measurements (Metrohm combination glass electrode) and leachate sampling followed by inductively coupled plasma atomic emission spectroscopy (ICP-AES) measurements of elemental Si, U, and Th concentrations. For each sample, 1.1 mL of the leaching solution was withdrawn and centrifuged at 12 000 rpm for 2 min. These conditions ensured the removal of colloids larger than 10 nm. Then 1 mL of the solution was diluted in at least 5 mL of 0.2 mol·L^{-1} HNO_3 solution for further ICP-AES analyses using a Spectro Arcos EOP device. For this purpose the spectrometer was calibrated with SPEX standard solutions. Fresh HCl solution was added to the dissolution reactors to maintain a constant leaching solution volume.

3. RESULTS AND DISCUSSION

3.1. Solid Characterizations. The qualitative analyses of PXRD patterns (Figure 1) revealed that the purification process yielded pure uranothorite single phases. In fact, all PXRD patterns exhibit the characteristic peaks of the tetragonal $I4_1/amd$ zircon-type structure, which correspond to the thorium–uranium(IV) mixed silicate (solid solution) as previously reported for $ThSiO_4$,[33,34] $USiO_4$,[19] and intermediate members of the uranothorite solid solution.[21,22]

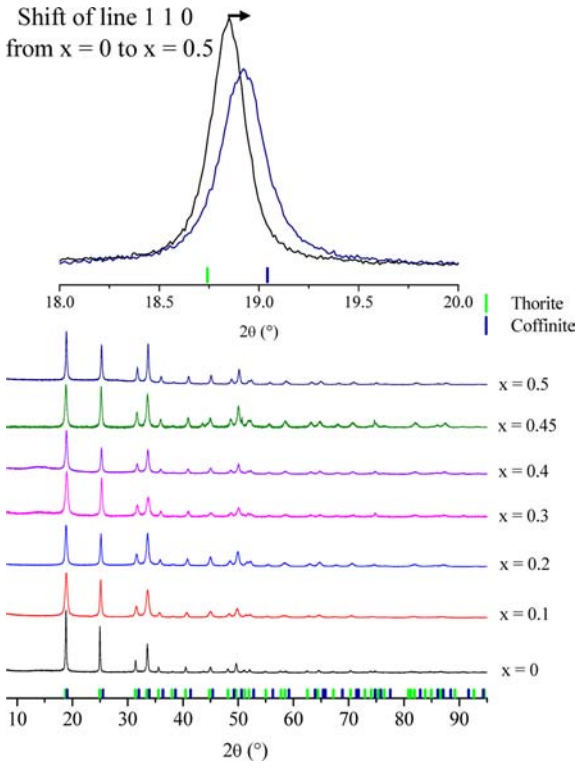

Figure 1. PXRD patterns of uranothorite solid solutions with various chemical compositions used in solubility experiments. Symbols represent Bragg position for thorite (green) and coffinite (blue) extracted, respectively, from JCPDS file #11-0419 and #11-0420.

Therefore, the Rietveld refinements of the recorded PXRD patterns were carried out by considering only the pure uranothorite phase free from other side products (oxides). Good agreements were observed between experimental and calculated data regardless of the sample composition. As an example, the Rietveld plot of sample with x = 0.2 is viewed in Figure 2. It led systematically to good reliability factors (R_{Bragg}, R_F) ranging between 5% and 8%.

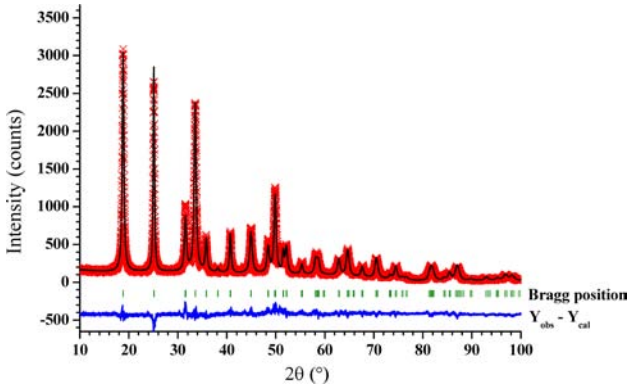

Figure 2. Observed pattern (red crosses), calculated pattern (black curve), and difference line (blue curve) for $Th_{0.8}U_{0.2}SiO_4$.

Regardless of the chemical composition, ESEM micrographs of the uranothorite solid solutions after purification (Figure 3) confirmed the presence of a single phase consisting of lens-shaped grains ranging in size from 120 ± 20 nm (x = 0.1) to 330 ± 70 nm (x = 0.5) as determined on almost 30 grains. The presence of secondary amorphous or gelatinous phases was not evidenced after the purification procedure. The size of the grains was found to increase with the uranium mole ratio, except for thorite that was constituted of larger grains than uranothorite with x = 0.1. However, the grain size variation could be not directly correlated to the U mole fraction, because the duration of the hydrothermal treatments was not always comparable (24 h for x = 0–0.3; 48 h for x = 0.4; 64 h for x = 0.45 and 0.5). Nevertheless, the variations in the specific surface area of the powders appeared to be related to the grain size (the sample with the lowest grain size, x = 0.1, presented the highest specific surface area).

dx.doi.org/10.1021/ic400272s | Inorg. Chem. 2013, 52, 6957–6968

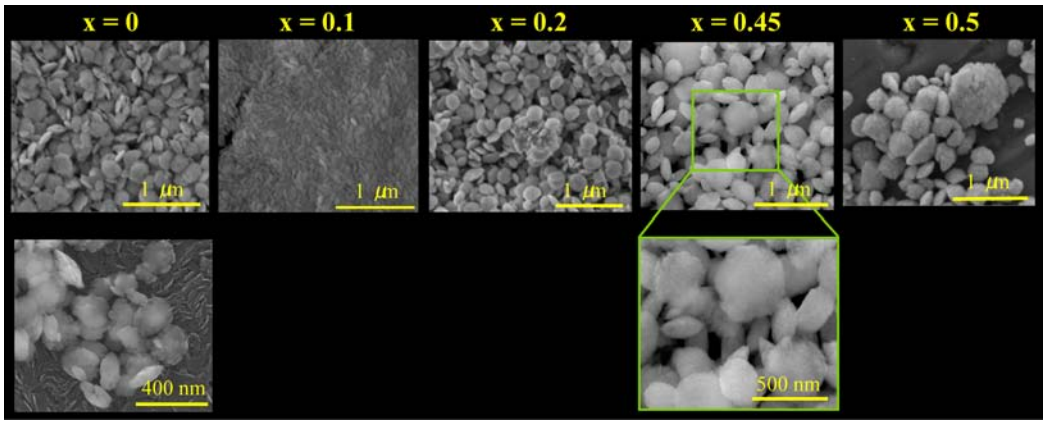

Figure 3. SEM micrographs of some of the uranothorite samples used in solubility experiments after purification.

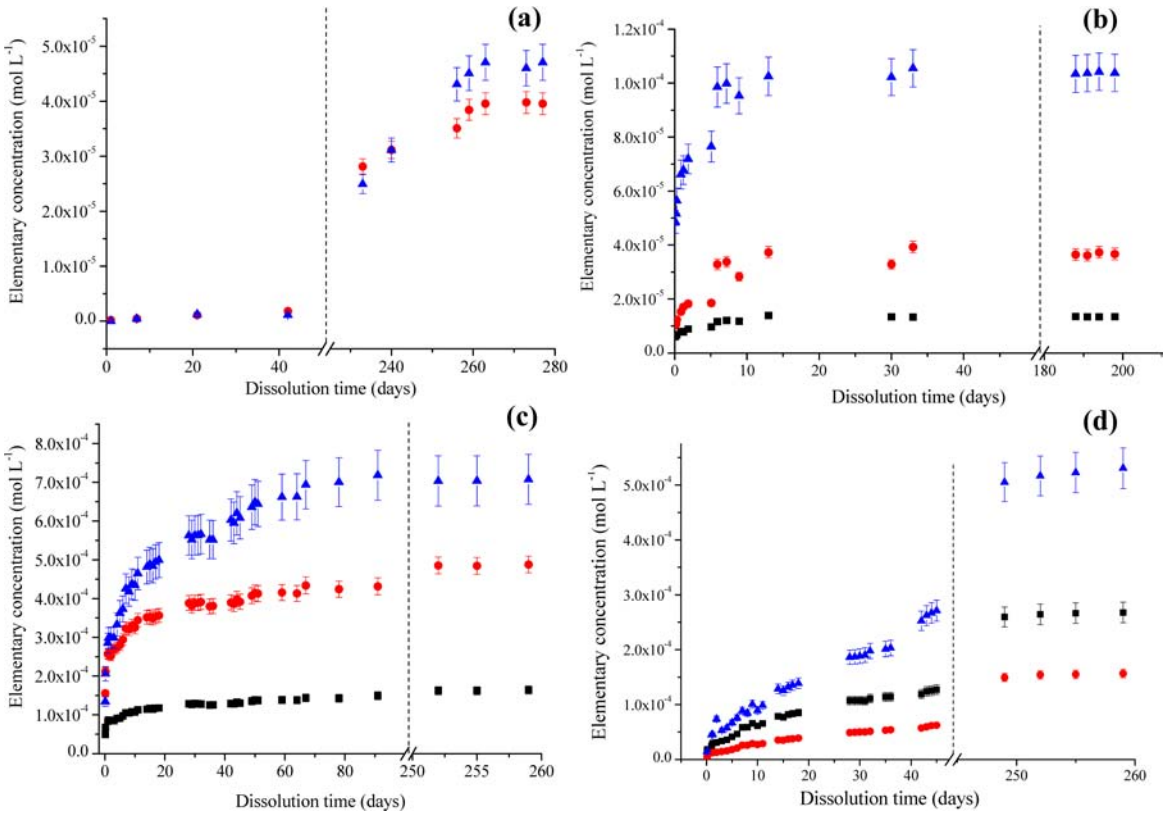

Figure 4. Evolution of the elemental concentrations (blue triangles, Si; red circles, Th; black squares, U) during the dissolution of (a) $ThSiO_4$, (b) $Th_{0.91}U_{0.09}SiO_4$, (c) $Th_{0.80}U_{0.20}SiO_4$, and (d) $Th_{0.49}U_{0.51}SiO_4$ in 0.1 mol L^{-1} HCl at 298 K under Ar atmosphere.

In a previous study, Costin et al.[22] gave evidence of the polycrystalline nature of such uranothorite grains. Indeed, the size of the crystallites (i.e., length of the coherent domains) determined from Rietveld refinement of the PXRD data was systematically found between 10 and 30 nm whatever the chemical composition considered, which is an order of magnitude smaller than the grain size.

X-EDS analyses were performed for each sample. The U, Th, and Si atomic fractions as well as An/Si ratios were determined (Table 1). The U/Th mole ratio of the mixed silicate was not strictly equal to that of the thorium−uranium chloride starting mixture. This was mainly due to the initial precipitation of side products, SiO_2 and thorium−uranium dioxide solid solutions. In addition, the good agreement on the composition of the mixed silicate phase from Rietveld refinement and the uranium mole fraction determined by X-EDS confirmed that the mixed silicate was the predominant phase whatever the composition of the solid solution after the purification process. Nevertheless, because the An/Si mole ratio differed slightly from 1, the presence of small amounts of impurities cannot be totally excluded. However, these phases, if present, were in such small amounts that they were not detected by PXRD and SEM.

3.2. Dissolution Experiments. The patterns of the elemental concentration variation obtained during dissolution experiments were used to determine equilibrium in solutions. For all the experiments carried out at 298 K, a plateau was reached within 190−260 days of leaching time (Figure 4).

The system was considered to be at equilibrium when the results of at least three consecutive analyses were in the range of two standard deviations. The composition of the solution at

dx.doi.org/10.1021/ic400272s | Inorg. Chem. 2013, 52, 6957−6968

Table 2. Composition of the Equilibrated Solutions from the Dissolution Experiments of Uranothorite Solid Solutions and Calculated Equilibrium Activities of Ions in Solution and Ion Activity Products

sample ID		mean total concentration in equilibrated solution					calculated activities			
x_{exp} (EDS)	T (K)	pH	[U] mol L^{-1}	[Th] mol L^{-1}	[Si] mol L^{-1}	I (mol L^{-1})	$\log(U^{4+})_{sss}$	$\log(Th^{4+})_{ss}$	$\log(H_4SiO_4)_{ss}$	log IAP
0	298	1.06		$(4.0 \pm 0.2) \times 10^{-5}$	$(4.7 \pm 0.2) \times 10^{-5}$	0.10		−5.59	−4.27	−5.62 ± 0.43
0.09	298	1.17	$(1.7 \pm 0.1) \times 10^{-5}$	$(7.7 \pm 0.2) \times 10^{-5}$	$(1.3 \pm 0.1) \times 10^{-4}$	0.09	−6.82	−5.44	−3.91	−4.80 ± 0.13
0.20	298	0.92	$(2.1 \pm 0.8) \times 10^{-4}$	$(6.3 \pm 0.3) \times 10^{-4}$	$(8.7 \pm 0.5) \times 10^{-4}$	0.13	−5.79	−4.63	−3.07	−4.25 ± 0.33
0.26	298	1.22	$(1.4 \pm 0.1) \times 10^{-4}$	$(2.3 \pm 0.1) \times 10^{-4}$	$(3.9 \pm 0.2) \times 10^{-4}$	0.09	−5.90	−4.95	−3.41	−3.80 ± 0.07
0.35	298	0.95	$(8.5 \pm 0.4) \times 10^{-4}$	$(1.44 \pm 0.07) \times 10^{-3}$	$(2.3 \pm 0.1) \times 10^{-3}$	0.12	−5.17	−4.25	−2.64	−3.40 ± 0.09
0.45	298	0.90	$(1.32 \pm 0.04) \times 10^{-3}$	$(1.19 \pm 0.06) \times 10^{-3}$	$(2.3 \pm 0.1) \times 10^{-3}$	0.12	−4.99	−4.33	−2.63	−3.66 ± 0.02
0.51	298	1.15	$(2.82 \pm 0.02) \times 10^{-4}$	$(1.63 \pm 0.02) \times 10^{-4}$	$(5.53 \pm 0.08) \times 10^{-4}$	0.10	−5.60	−5.14	−3.26	−4.02 ± 0.02
0	313	1.10		$(5.8 \pm 0.2) \times 10^{-5}$	$(9.3 \pm 0.3) \times 10^{-5}$	0.10		−5.62	−4.03	−5.41 ± 0.15
0.2	313	1.20	$(1.13 \pm 0.04) \times 10^{-4}$	$(2.57 \pm 0.05) \times 10^{-4}$	$(5.58 \pm 0.06) \times 10^{-4}$	0.11	−6.14	−4.99	−3.25	−3.67 ± 0.15
0.45	313	1.00	$(1.10 \pm 0.02) \times 10^{-3}$	$(8.2 \pm 0.2) \times 10^{-4}$	$(2.29 \pm 0.05) \times 10^{-3}$	0.14	−5.19	−4.55	−2.64	−3.47 ± 0.05
0	332	1.10		$(1.3 \pm 0.1) \times 10^{-4}$	$(2.0 \pm 0.7) \times 10^{-4}$	0.10		−5.34	−3.69	−4.63 ± 0.26
0.2	332	1.11	$(2.9 \pm 0.2) \times 10^{-4}$	$(6.9 \pm 0.2) \times 10^{-4}$	$(1.09 \pm 0.02) \times 10^{-3}$	0.11	−6.05	−4.62	−2.96	−3.43 ± 0.10
0.45	332	1.07	$(1.18 \pm 0.02) \times 10^{-3}$	$(8.7 \pm 0.3) \times 10^{-4}$	$(3.7 \pm 0.1) \times 10^{-3}$	0.11	−5.47	−4.52	−2.43	−3.09 ± 0.13
0	346	0.95		$(8.3 \pm 0.2) \times 10^{-4}$	$(7.4 \pm 0.2) \times 10^{-4}$	0.12		−4.60	−3.13	−3.92 ± 0.17
0.2	346	1.10	$(6.4 \pm 0.2) \times 10^{-4}$	$(1.49 \pm 0.04) \times 10^{-3}$	$(2.21 \pm 0.1) \times 10^{-3}$	0.12	−5.97	−4.36	−2.65	−2.94 ± 0.18
0.45	346	1.05	$(3.16 \pm 0.09) \times 10^{-3}$	$(1.71 \pm 0.05) \times 10^{-3}$	$(5.2 \pm 0.2) \times 10^{-3}$	0.14	−5.31	−4.33	−2.28	−2.84 ± 0.17

saturation with respect to the solid phase was then calculated as the average of consecutive analyses that were not significantly different from each other. Finally, the average composition of the solutions equilibrated with the solids as well as two standard deviations of duplicate experiments are listed in Table 2. The pH of the solutions at equilibrium were measured at least three times and the average values are indicated in Table 2.

Dissolution experiments at 313, 332, and 346 K were also performed for three solid solutions: $x_{exp} = 0$, $x_{exp} = 0.2$ and $x_{exp} = 0.45$. As an example, the elemental concentrations are plotted versus the dissolution time for $Th_{0.55}U_{0.45}SiO_4$ and different temperatures in Figure 5.

ESEM examination of uranothorite solid solutions during dissolution experiments revealed that the morphology of the grains was unmodified during the dissolution (Figure 6). However, the grain size decreased after 2 months in the dissolution media, revealing the crystallites and leading to an increase in the surface roughness of the grains. These observations gave no evidence of neoformed phases.

Figure 7a shows the final elemental concentrations determined in solution when equilibrium is reached at 298 K. At this temperature, there is an apparent increase of the solubility for $Th_{0.65}U_{0.35}SiO_4$ and $Th_{0.55}U_{0.45}SiO_4$. Then the concentrations seemed to decrease. Such behavior was already observed in the case of solid solutions with end members of similar solubility.[35] The stoichiometry of the solutions equilibrated in the dissolution experiments is shown in Figure 7b. The (U+Th)/Si mole ratio in equilibrium solutions was consistent with the solid stoichiometry. However, Figure 7b reveals a slight deficit in Th in solution compared with the solid composition. Because the precipitation of a Th-enriched neoformed phase was not observed by ESEM, this bias might be explained partly by the accuracy of the elemental concentration analysis and solid composition measurement by X-EDS. Nevertheless, the results were used to perform a first estimation of the solubility of uranothorite solid solutions.

The dissolution of uranothorite solid solutions can be written as in the general equation[36]

$$Th_{1-x}U_xSiO_4(s) + 4H^+ \leftrightarrows (1-x)Th^{4+}(aq) + xU^{4+}(aq) + H_4SiO_4(aq) \quad (3)$$

Following eq 3, the experimental ion activity products (IAPs) determined for uranothorite solid solutions were calculated using the general equation

$$IAP = (U^{4+})_{ss}^{\ x}(Th^{4+})_{ss}^{\ 1-x}(H_4SiO_4)_{ss}(H^+)_{ss}^{\ -4} \quad (4)$$

where $()_{ss}$ denotes the activity of ions in solution when stoichiometric saturation was reached.

From the elemental concentrations, pH value, and partial pressure of O_2 controlled in the glovebox, the ion activities were calculated with the geochemical speciation model PHREEQC-2,[37] using the LLNL thermodynamic database.[38,39] The thermodynamic data used for the calculations are listed in Table S1 of the Supporting Information. PHREEQC-2 calculates activity corrections using the Davies equation:

$$\log(\gamma_i) = -AZ_i^2\left(\frac{\sqrt{I}}{1+\sqrt{I}} - 0.3I\right) \quad (5)$$

where γ_i is the activity coefficient for ion i, A is a constant dependent on the dielectric constant of water and temperature, Z corresponds to the charge of the ion, and I is the ionic strength of the solution. The ionic strength did not exceed 0.1 mol L^{-1} for all the experiments performed. According to the literature, the use of the Davies equation for activity corrections is acceptable under these conditions.[13,40]

The calculated IAPs of solids from the dissolution experiments are listed in Table 2. Errors reported for the IAP values are the total standard deviation propagating the error in the elemental concentrations at saturation of the solution.

3.3. Thermodynamic Properties of Uranothorite Solid Solutions. In the case of the binary solid solution (Th,U)SiO_4, in which Th^{4+} and U^{4+} substitute for each other, the solid phase consists of two components, $ThSiO_4$ and $USiO_4$, and two reactions are required to describe the dissolution, namely,

$$ThSiO_4(s) + 4H^+ \leftrightarrows Th^{4+}(aq) + H_4SiO_4(aq) \quad (6)$$

$$USiO_4(s) + 4H^+ \leftrightarrows U^{4+}(aq) + H_4SiO_4(aq) \quad (7)$$

According to the law of mass action, the equilibrium distribution between the species in eqs 6 and 7 is given by the following two equation system:[41−43]

dx.doi.org/10.1021/ic400272s | Inorg. Chem. 2013, 52, 6957−6968

$$\begin{cases} K_{S,Th} = \dfrac{(Th^{4+})(H_4SiO_4)}{(H^+)^4 a_{ThSiO_4}} \\ K_{S,U} = \dfrac{(U^{4+})(H_4SiO_4)}{(H^+)^4 a_{USiO_4}} \end{cases} \quad (8)$$

where a_{AnSiO_4} (An = Th or U) denotes the activity of each component of the binary solid solution. The activity is dimensionless and is given by:

$$a_{ThSiO_4} = \gamma_{ThSiO_4}(1 - x) \quad \text{or} \quad a_{USiO_4} = \gamma_{USiO_4} x \quad (9)$$

where γ_{AnSiO_4} (An = Th or U) is the activity coefficient of each component of the binary solid solution. For an ideal solid solution, $\gamma_{AnSiO_4} = 1$ for each component of the solid solution.

It is noteworthy that $K_{S,U} = ((U^{4+})(H_4SiO_4))/((H^+)^4 x)$ becomes the solubility product of coffinite end member, $^*K_{S,USiO_4}$ for the particular case $x = 1$, and $K_{S,Th} = ((Th^{4+})(H_4SiO_4))/((H^+)^4(1 - x))$ becomes the solubility product of thorite end member, $^*K_{S,ThSiO_4}$ for the particular case $x = 0$.

The system of two eqs 8 describes thermodynamic equilibrium in the binary solid solution (Th,U)SiO_4 aqueous solution system. Thorstenson and Plummer (1977)[44] argued that in geological environments, such systems barely achieve thermodynamic equilibrium in an observable time scale. However, the rate of dissolution is almost zero when the aqueous phase reaches a point of stoichiometric saturation with respect to the solid phase. According to Thorstenson and Plummer (1977),[44] the stoichiometric saturation state refers to a metastable equilibrium state between the aqueous phase and the solid solution "in situations where owing to kinetic restrictions, the composition of the solid phase remains invariant, even though the solid phase may be a part of continuous compositional series". Following this approach, an equilibrium constant expression for the congruent dissolution reaction 3 of a solid solution of composition $Th_{1-x}U_xSiO_4$ is:

$$^*K_{st} = \frac{(U^{4+})_{ss}^{\ x}(Th^{4+})_{ss}^{\ 1-x}(H_4SiO_4)_{ss}}{(H^+)^4} \quad (10)$$

Note that our experimental raw results appeared to be consistent with stoichiometric dissolution: this can also be used as an experimental observation to directly derive the above equations, which finally do not need the above justifications proposed by Thorstenson and Plummer. In eq 10, the solid-phase activity becomes equal to unity, since the activity of a single component is equal to one by definition.[45,46] The IAP at stoichiometric saturation of the solution becomes equal to the stoichiometric solubility product defined by eq 10.[36,41,44−46]

This stoichiometric solubility product can be expressed in terms of the solubility product of the end members:

$$^*K_{st} = (K_{S,U}\gamma_{USiO_4}x)^x(K_{S,Th}\gamma_{ThSiO_4}(1 - x))^{1-x} \quad (11)$$

The value of $^*K_{st}$ will thus vary as a function of the solid solution composition. Thermodynamic equilibrium corresponds to a state described by the system of eqs 8 linking the activities of the components in the solid phase to the activities of the constituent ions in the aqueous solution. These two equations have been reduced by linear combination to eq 11 defining the stoichiometric solubility product. Thus, as already pointed out by Dandurand and Schott (1980)[47] and then Glynn and Reardon (1990),[36] the constraint that IAP = K_{st} is a necessary but not sufficient condition for thermodynamic equilibrium. A second equation must be verified at equilibrium. One of the most frequently used is the partitioning of the substituting ions in the solid solution−aqueous solution system through the so-called distribution coefficient,[48] D_U:

$$D_U = \frac{(Th^{4+})_{ss}x}{(U^{4+})_{ss}(1 - x)} \quad (12)$$

D_U is also derived from the system 8 of the two basic conditions defining thermodynamic equilibrium in the binary solid solution−aqueous solution system. Therefore, the distribution coefficient can be expressed in terms of the end member solubility products:

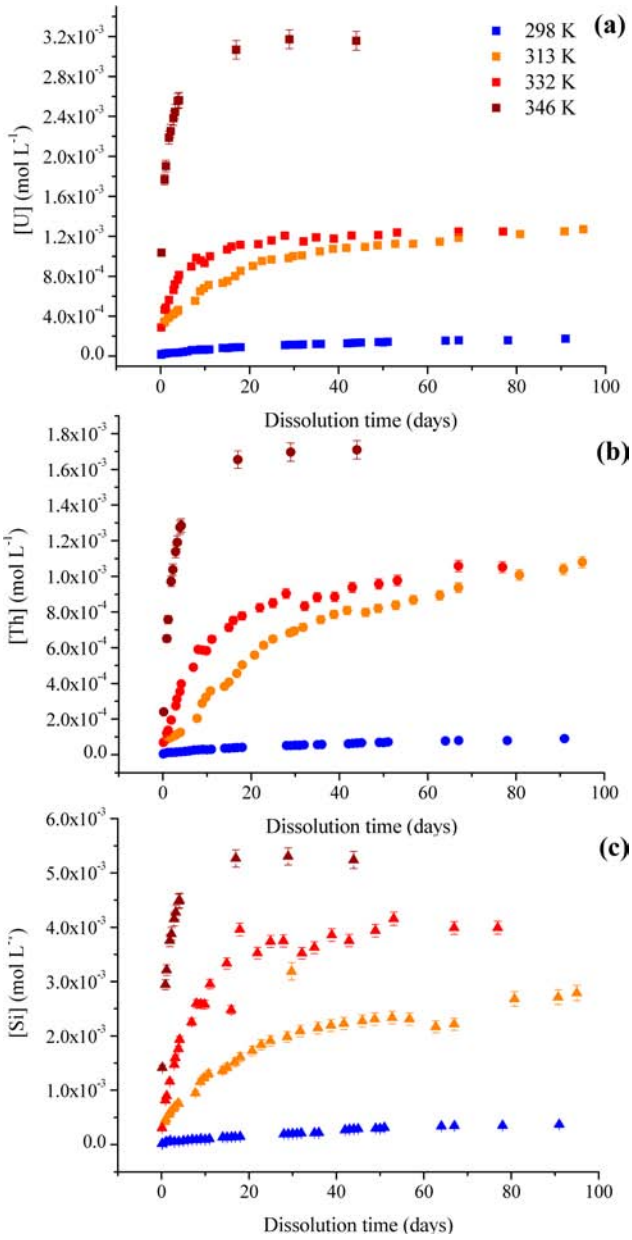

Figure 5. Evolution of the total concentration of (a) uranium, (b) thorium, and (c) silicon during the dissolution of $Th_{0.55}U_{0.45}SiO_4$ in 0.1 M HCl at 298 K (blue); 313 K (orange); 332 K (red), and 346 K (brown) under Ar atmosphere.

dx.doi.org/10.1021/ic400272s | Inorg. Chem. 2013, 52, 6957−6968

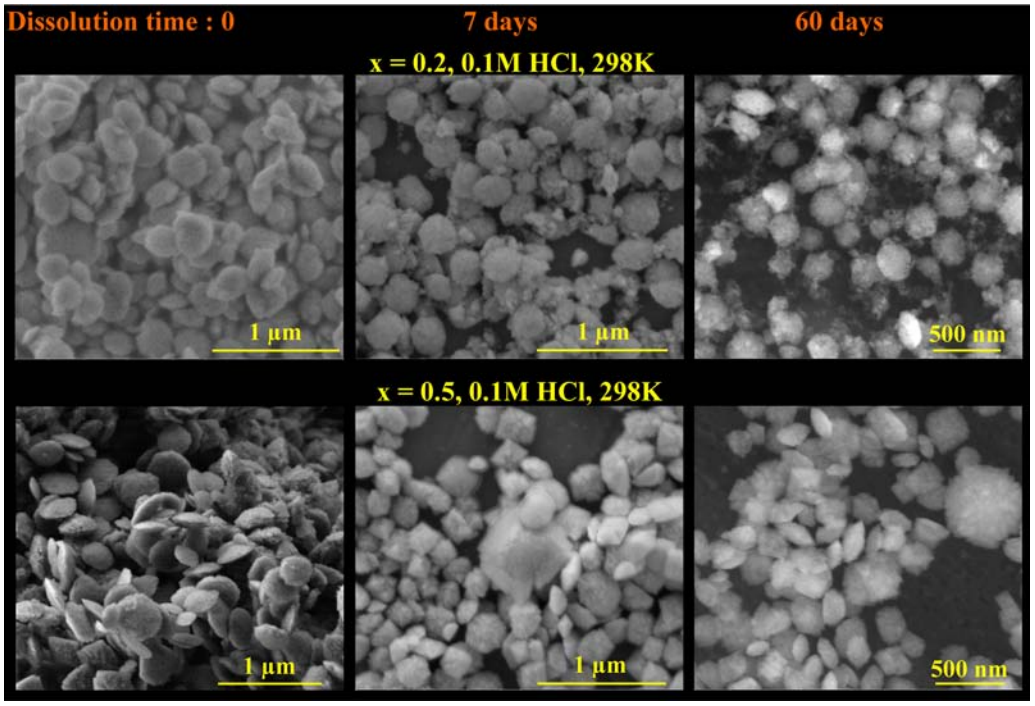

Figure 6. SEM micrographs of $Th_{0.8}U_{0.2}SiO_4$ and $Th_{0.49}U_{0.51}SiO_4$. Initial stage and samples observed after 7 days and 60 days of dissolution in 0.1 mol·L^{-1} HCl at 298 K under Ar atmosphere.

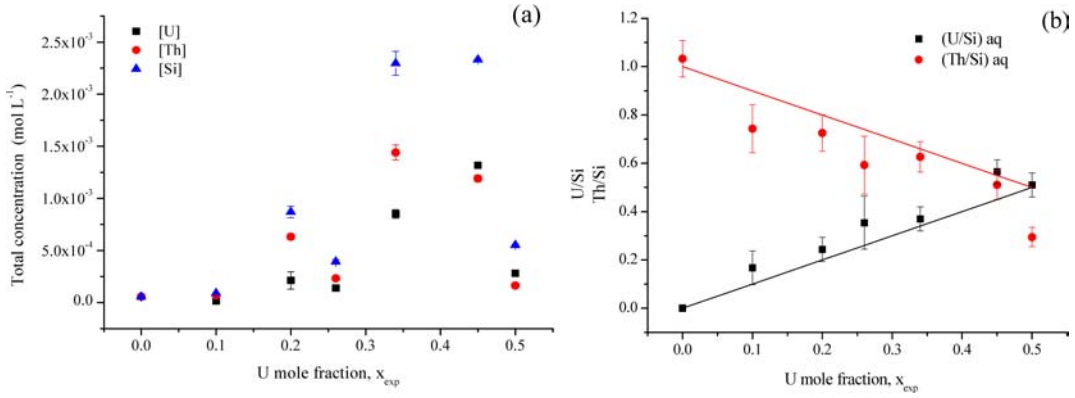

Figure 7. (a) Variation of the elemental concentrations (blue triangles, Si; red circles, Th; black squares, U) determined by ICP-AES versus the composition of uranothorite solid solutions at equilibrium with 0.1 mol·L^{-1} HCl at 298 K under Ar atmosphere. (b) Stoichiometry of the equilibrated solutions versus the sample chemical composition. Solid lines stand for the mole ratio of elements in the uranothorite samples.

$$D_U = \frac{K_{S,Th}\gamma_{ThSiO_4}}{K_{S,U}\gamma_{USiO_4}} \quad (13)$$

Distribution coefficients can be determined, provided the solid solution composition is invariant and the activity coefficients of Th^{4+} and U^{4+} are known. They can be interpreted in terms of either an end member solubility product or an activity coefficient for the components of the solid solution (γ_{AnSiO_4}).[46] Indeed, because both γ_{ThSiO_4} and γ_{USiO_4} depend on the uranothorite solid solution composition, the distribution coefficient at equilibrium defined in eq 13 is not constant but appears as a function that can change with composition, except in the case of ideal solid solutions where this coefficient is equal to the ratio of the solubility constants of the end members.

The values of D_U determined by dissolution experiments at 298 K are reported in Table 3 and Figure 8a. Considering the uncertainties associated with experimental measurements of elemental concentrations, the values of D_U were not significantly different. As expected in the case of an ideal solid solution, D_U takes a constant value for the investigated composition range. The obtained values of D_U greater than 1 indicated that U atoms are preferentially incorporated into the solid phase due to the slightly lower solubility of coffinite compared with thorite.

Assuming that the activity coefficients in the solid phase were equal to unity, a value of $^*K_{S,USiO_4}$ was deduced from each independent value of D_U. The values calculated from distribution coefficients assuming an ideal solid solution are also reported in Figure 8b. The solubility of thorite and coffinite had never been directly measured from solubility experiments. The reported values for the solubility constants of coffinite listed in Table 4 have been derived from molecular calculations or by analogy with other orthosilicates.[16,17,49] The value selected by Grenthe[12] in the NEA TDB project is based on the hypothesis initially made

dx.doi.org/10.1021/ic400272s | Inorg. Chem. 2013, 52, 6957−6968

Table 3. Stoichiometric Solubility Constants of Uranothorite Solid Solutions, Standard Gibbs Free Energy Associated with the Dissolution Reaction, and Distribution Coefficients[a]

x_{exp}	T (K)	$^*K_{S,ThSiO_4}$ or $^*K_{st}$	$\Delta_R G°$ (kJ mol^{-1})	D_U	$^*K_{S,USiO_4}$
0	298	$(2.40 \pm 0.48) \times 10^{-6}$	32.1 ± 0.6		
0.09	298	$(1.97 \pm 0.22) \times 10^{-5}$	26.9 ± 0.4	2.7 ± 0.6	$(9 \pm 2) \times 10^{-7}$
0.20	298	$(5.56 \pm 1.85) \times 10^{-5}$	24.3 ± 0.9	3.6 ± 0.4	$(7 \pm 1) \times 10^{-7}$
0.26	298	$(1.57 \pm 0.13) \times 10^{-5}$	21.7 ± 0.3	3.1 ± 0.3	$(8 \pm 1) \times 10^{-7}$
0.35	298	$(3.98 \pm 1.19) \times 10^{-4}$	19.4 ± 0.8	4.3 ± 0.4	$(5.5 \pm 0.8) \times 10^{-7}$
0.45	298	$(2.20 \pm 0.16) \times 10^{-4}$	20.9 ± 0.4	3.7 ± 0.3	$(6.5 \pm 0.9) \times 10^{-7}$
0.51	298	$(9.52 \pm 1.43) \times 10^{-5}$	23.0 ± 0.4	2.9 ± 0.3	$(8 \pm 1) \times 10^{-7}$
0	313	$(3.89 \pm 0.58) \times 10^{-6}$	32.4 ± 0.2		
0.20	313	$(2.13 \pm 0.32) \times 10^{-4}$	22.0 ± 0.2	3.5 ± 0.4	$(1.1 \pm 0.1) \times 10^{-6}$
0.45	313	$(3.37 \pm 0.17) \times 10^{-4}$	20.8 ± 0.1	3.4 ± 0.3	$(1.2 \pm 0.1) \times 10^{-6}$
0	332	$(2.37 \pm 0.62) \times 10^{-5}$	29.4 ± 0.3		
0.20	332	$(3.76 \pm 0.38) \times 10^{-4}$	21.8 ± 0.1	6.7 ± 0.8	$(3.5 \pm 0.4) \times 10^{-6}$
0.45	332	$(8.2 \pm 1.1) \times 10^{-4}$	19.6 ± 0.2	7.0 ± 0.6	$(3.4 \pm 0.3) \times 10^{-6}$
0	346	$(1.19 \pm 0.20) \times 10^{-4}$	26.0 ± 0.2		
0.2	346	$(1.16 \pm 0.21) \times 10^{-3}$	19.5 ± 0.2	10.3 ± 1.3	$(1.2 \pm 0.1) \times 10^{-5}$
0.45	346	$(1.43 \pm 0.24) \times 10^{-3}$	18.8 ± 0.2	7.5 ± 0.7	$(1.6 \pm 0.2) \times 10^{-5}$

[a]Solubility constants of coffinite are deduced from the distribution coefficients.

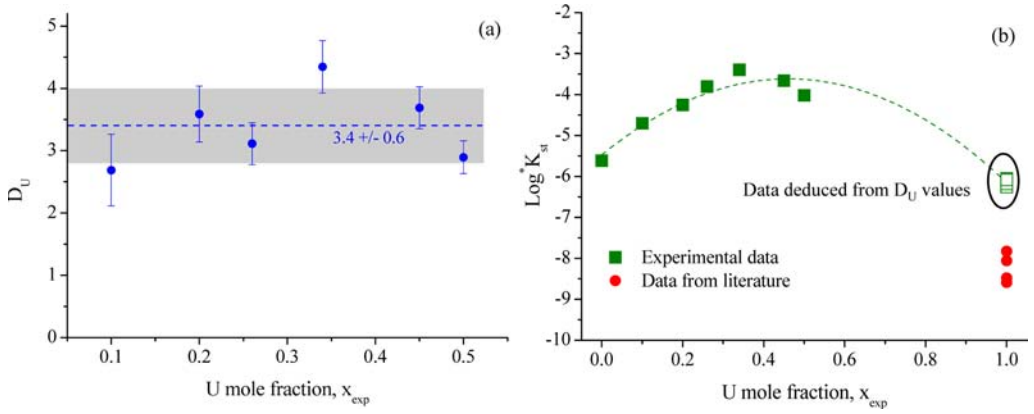

Figure 8. (a) Variation of the distribution coefficient D_U (blue circles) with the uranium loading of uranothorite solid solutions determined at stoichiometric saturation of the solution. (b) Variation of the stoichiometric solubility constant (green squares) along the uranothorite series determined by undersaturation experiment at 298 K under Ar atmosphere with extrapolation to the coffinite solubility constant. The red symbols (red circles) correspond to published solubility constants of coffinite (values from literature with associated references are indicated in Table 4).

Table 4. Standard Gibbs free energy, enthalpy and entropy associated with the formation of uranothorites determined in this work and compared with published values

phase	log $^*K_S$ or log $^*K_{st}$	$\Delta_f G°$ (kJ mol^{-1})	$\Delta_f H°$ (kJ mol^{-1})	$\Delta_f S°$ (J mol^{-1} K^{-1})
$USiO_4$	−7.83[14]	−1883.6[14]	−2001.4 ± 4.7[14]	
	−8.59[16]	−1886 ± 6[16]		
	−8.064 ± 0.434[12,13]	−1883.6 ± 4.0[12,13]	−1991.326 ± 5.367[12,13]	−292 ± 12[12,13]
	−8.48[50]	−1835.23[50]		
	−33.36[17]	−2028[17]		
	−6.1 ± 0.2	−1872 ± 6	−2101 ± 32	−767 ± 80
$ThSiO_4$		−2050.3 ± 3.9[51]	−2117.5 ± 4.2[52,53]	
	−5.62 ± 0.08	−2044 ± 11	−2282 ± 50	−795 ± 110
$Th_{0.8}U_{0.2}SiO_4$	−4.3 ± 0.2	−2001 ± 12	−2241 ± 24	−804 ± 50
$Th_{0.55}U_{0.45}SiO_4$	−3.66 ± 0.04	−1956 ± 10	−2194 ± 15	−801 ± 30

by Langmuir,[14] who assumed that uraninite and coffinite are in equilibrium at low temperatures and control the groundwater dissolved silica concentration at a level of 10^{-3} mol·L^{-1}. The average value determined in this work, log $^*K_{S,USiO_4} = -6.1 \pm 0.2$, is higher than that previously reported. Thus, the solution in equilibrium with coffinite at circumneutral pH under anoxic conditions is slightly supersaturated with regard to uraninite at low temperature and undersaturated with regard to chalcedony (and *a fortiori* to quartz), with a H_4SiO_4(aq) concentration of 10^{-5} mol·L^{-1}.

The calculated values for the stoichiometric solubility products of the uranothorite solid solutions, solubility products of coffinite end member, and the corresponding standard Gibbs free energy associated with the dissolution reaction are also reported in Table 3. Because the dissolution of the uranothorite solid

dx.doi.org/10.1021/ic400272s | Inorg. Chem. 2013, 52, 6957−6968

solutions was congruent and the dissolution kinetics were slow, the composition of the silicate phases remained invariant. The conditions to use the Thorstenson and Plummer stoichiometric saturation model were thus fulfilled. The standard Gibbs free energy associated with reaction 1 was then determined with the following expression:[36,44]

$$\Delta_R G^\circ(T) = -RT \ln {}^*K_{st}(T) \quad (14)$$

where R is the universal gas constant and T is the absolute temperature.

The reported uncertainties were calculated by propagating the experimental errors associated either with the determination of the activities of cations in solution at stoichiometric saturation or with the determination of uranium and thorium mole fractions in the solid solution by X-EDS.

As shown in Figure 8b, the stoichiometric solubility product of uranothorite solid solutions (following eq 9) reaches a maximum value for $x_{exp} = 0.45 \pm 0.05$. In terms of the standard Gibbs free energy of dissolution (Table 3), uranothorite solid solutions dissolve more spontaneously than both end members. From Glynn and Reardon (1990),[36] the standard Gibbs free energy associated with the congruent dissolution reaction of a real solid solution can be expressed in terms of the standard Gibbs free energy associated with the dissolution of an ideal solid solution, $\Delta_R G^{\circ,id}$ with the same composition and the excess free energy of mixing, ΔG_E according to the following relation:

$$\Delta_R G^\circ(T) = \Delta_R G^{\circ,id}(T) - \Delta G_E(T) \quad (15)$$

Because the two end members are isomorphic, the mixing properties can be represented by single curves across the whole composition range.[45] From the results obtained for uranothorite solid solutions (Figure 8b), the excess energy of mixing can be well described by a function that is symmetric around $x_{exp} = 0.5$. In such a case, the solid solution is termed "regular". In addition, the linear variation of the molar volume of mixing evidenced by Costin et al.[22] or by Fuchs and Hoekstra[15] indicates that the excess molar volume of mixing (ΔV_E) is equal to zero. Assuming perfect random substitution of Th(IV) and U(IV) in the solid solution led to $\Delta S_E = 0$. This special case corresponds to "strictly regular" solid solutions for which the only contribution to the excess free energy of mixing comes from the enthalpy of mixing, ΔH_M.[54] This requirement also implies that ΔG_E is independent of the temperature. If thermodynamic equilibrium was reached, the experimental results indicate that the solid solution is less stable than the end members at 298 K (the more stable is coffinite), which could be attributed to the nonideality of the uranothorite solid solution as previously discussed. However, the calculated values of D_U did not vary with the solid composition, as reported for ideal solid solutions. Thus, the dissolution process of uranothorite solid solutions might have reached a metastable equilibrium, which could explain this result. Indeed, from thermodynamic properties, coffinite should precipitate during the experiment and thus a deficit in uranium in solution should be observed. The experimental results indicate the opposite (a slight deficit in Th was observed). Thus, coffinite did not precipitate probably owing to kinetic restrictions. According to Thorstenson and Plummer,[44] this situation still allows using eq 14 in the stoichiometric saturation model.

If the variation of $\Delta_R H^\circ$ and $\Delta_R S^\circ$ in the studied temperature range can be neglected, which is commonly admitted for small temperature ranges, then the standard Gibbs free energy of the dissolution reaction can be calculated from the standard enthalpy and standard entropy of reaction by

$$\Delta_R G^\circ(T) = \Delta_R H^\circ - T\Delta_R S^\circ \quad (16)$$

Combining eq 11 and eq 12 leads to

$$\ln {}^*K_{st} = \frac{-\Delta_R H^\circ}{RT} + \frac{-\Delta_R S^\circ}{R} \quad (17)$$

The variation of the stoichiometric solubility constants of thorite, $Th_{0.8}U_{0.2}SiO_4$, $Th_{0.56}U_{0.44}SiO_4$ and coffinite versus the reciprocal of the temperature is plotted in Figure 9. The linear

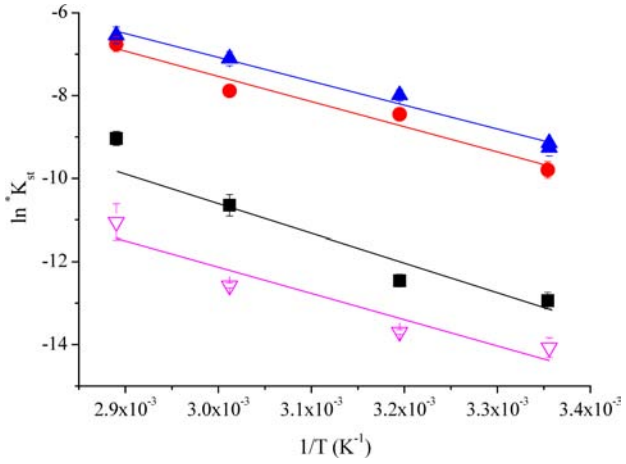

Figure 9. Variation of stoichiometric solubility constant of thorite (black squares), $Th_{0.8}U_{0.2}SiO_4$ (red circles), and $Th_{0.56}U_{0.44}SiO_4$ (blue triangles) and the solubility constant of coffinite (pink open triangles) versus the reciprocal of the temperature. The linear regression allowed determination of the standard enthalpy of reaction of each solid, $\Delta_R H^\circ$, listed in Table 5.

regression allowed determining the standard enthalpy of reaction of each solid, $\Delta_R H^\circ$, as well as the standard entropy of reaction of each solid, $\Delta_R S^\circ$, listed in Table 5.

The calculated values of $\Delta_R G^\circ(T)$, $\Delta_R H^\circ$, and $\Delta_R S^\circ$ for reaction 1 were used in Hess's law (eq 18) to determine the thermodynamic data ($\Delta_f G^\circ$, $\Delta_f H^\circ$, and $\Delta_f S^\circ$) associated with the formation of uranothorite solid solutions:

$$\Delta_R X^\circ = \sum_i \nu_i \Delta_f X^\circ \quad (18)$$

where $X = G$, H, or S and ν_i are the algebraic stoichiometric coefficients of the reactants (negative) and products (positive) of the reaction.

The obtained values, compared with published values for coffinite and thorite, are listed in Table 4. Considering the uncertainty associated with the standard free energy of formation of coffinite and thorite determined in this work, the values obtained were in good agreement with previous published values. The standard enthalpy and standard entropy of formation of thorite, coffinite, and uranothorite solid solutions are also listed in Table 4 as a first estimation. Nevertheless, the values obtained are subject to large uncertainties.

The standard Gibbs free energy of formation of uranothorite solid solutions increases with the uranium mole fraction. The apparent contradiction in the fact that coffinite dissolves less spontaneously than thorite (${}^*K_{S,USiO_4} < {}^*K_{S,ThSiO_4}$) and the higher value of the standard Gibbs free energy of formation of coffinite ($\Delta_f G^\circ = -1872 \pm 43$ kJ·mol^{-1}) compared with thorite (-2044 ± 54 kJ·mol^{-1}) is explained by the difference in the $\Delta_f G^\circ$ of the

dx.doi.org/10.1021/ic400272s | Inorg. Chem. 2013, 52, 6957−6968

Table 5. Equilibrium Constants of the Dissolution and "Uranothoritization" Reactions Calculated from the Solubility Experiments and Thermodynamic Data Reported as Supporting Information (Table S2)

reaction stoichiometry	log K(298 K)	$\Delta_R G°$(298K) (kJ mol^{-1})	$\Delta_R H°$ (kJ mol^{-1})	$\Delta_R S°$ (J K^{-1} mol^{-1})
Uranothorite Dissolution				
$ThSiO_4 + 4H^+ \leftrightarrows Th^{4+} + H_4SiO_4$	−5.6 ± 0.2	32.1 ± 0.9	56 ± 16	80 ± 52
$Th_{0.8}U_{0.2}SiO_4 + 4H^+ \leftrightarrows 0.2U^{4+} + 0.8Th^{4+} + H_4SiO_4$	−4.25 ± 0.18	24.3 ± 0.9	51 ± 7	89 ± 21
$Th_{0.55}U_{0.45}SiO_4 + 4H^+ \leftrightarrows 0.45U^{4+} + 0.55Th^{4+} + H_4SiO_4$	−3.66 ± 0.07	20.9 ± 0.3	48 ± 3	85 ± 10
$USiO_4 + 4H^+ \leftrightarrows U^{4+} + H_4SiO_4$	−6.1 ± 0.2	35.0 ± 0.9	53 ± 12	57 ± 36
"Uranothoritization"				
	log K(298 K)		$\Delta_R G°$(298K) (kJ mol^{-1})	
$ThO_{2(cr)} + SiO_{2(cr)} \leftrightarrows ThSiO_{4(cr)}$	3.4 ± 0.7		−19 ± 5.5	−25 ± 5[51]
$0.2UO_{2(cr)} + 0.8ThO_{2(cr)} + SiO_{2(cr)} \leftrightarrows Th_{0.8}U_{0.2}SiO_4$	0.7 ± 0.1		−4 ± 5	
$0.45UO_{2(cr)} + 0.55ThO_{2(cr)} + SiO_{2(cr)} \leftrightarrows Th_{0.55}U_{0.45}SiO_4$	−1.5 ± 0.2		9 ± 4	
$UO_{2(cr)} \pm SiO_{2(cr)} \leftrightarrows USiO_{4(cr)}$	−2.8 ± 0.5		16 ± 3	−4.5 ± 6.4[14]

substituting cations:[13] $\Delta_f G°(Th^{4+}) = -704.78 \pm 5.3$ kJ·mol^{-1}, whereas $\Delta_f G°(U^{4+}) = -529.86 \pm 1.76$ kJ·mol^{-1}. The values of the standard enthalpy of formation of uranothorite solid solutions are not significantly different nor is the standard entropy of formation.

Finally, the thermodynamic values associated with the formation of uranothorite solid solutions were used in Hess's law to estimate the standard free energy at 298 K of the "uranothoritization" reaction 19:

$$x\mathrm{UO_2(cr)} + (1-x)\mathrm{ThO_2(cr)} + \mathrm{SiO_2(cr)} \leftrightarrows \mathrm{Th_{1-x}U_xSiO_4(cr)} \quad (19)$$

The tabulated values of $\Delta_f G°$, $\Delta_f H°$, and $\Delta_f S°$ of the species involved in reactions 3 and 19 were taken from the NEA TDB II[13] and indicated in Table S2 of the Supporting Information.

The variation of the calculated values of the standard Gibbs free energy of "uranothoritization" reaction 19 at 298 K with the uranium mole fraction are presented in Figure 10a. These results indicate that the stability of uranothorite solid solutions at 298 K decreases with the uranium loading. The formation of uranothorite solid solution is thermodynamically favored for uranium mole fractions below 0.26. Above this value, the mixture of uranothorianite and silica becomes more stable. This observation is in good agreement with the results obtained by Mumpton and Roy[55] who showed that thorite is more stable than the silica−thorianite mixture below 1200 °C, when thorite was transformed to huttonite. The only attempt to determine the standard Gibbs free energy of formation of thorite was made by Schuiling et al. (1976).[51] The estimated value was $\Delta_f G° = -2050.3 \pm 3.9$ kJ mol^{-1}. This led to the value of -25 ± 5 kJ mol^{-1} for the standard free energy of reaction from binary oxides at 298 K. Considering the uncertainties, this is in agreement with the value obtained in this work: $\Delta_R G°(298\ K) = -19.0 \pm 5.5$ kJ mol^{-1}. Coffinite is less stable under standard conditions than the silica−uraninite mixture with $\Delta_R G°(298\ K) = 16 \pm 3$ kJ·mol^{-1}. This is in contradiction with the finding of Langmuir (1978),[14] who estimated that the standard free energy of the reaction of formation of $USiO_4$ from binary oxides at 298 K was -4.5 ± 6.4 kJ·mol^{-1}. In fact, the value obtained for the standard Gibbs free energy of the reaction of formation of $USiO_4$ from binary oxides at 298 K is not accurate enough to make a conclusion on the relative stability of these phases. The results obtained in this study give the first experimental evidence that coffinite is less stable than the uraninite and silica mixture at low temperature. In addition, the low value of the equilibrium constant obtained for the coffinitization reaction (log K(298 K) = −2.8 ± 0.5) indicates that this equilibrium might be easily reversed to favor the formation of coffinite as a function of temperature and pressure.

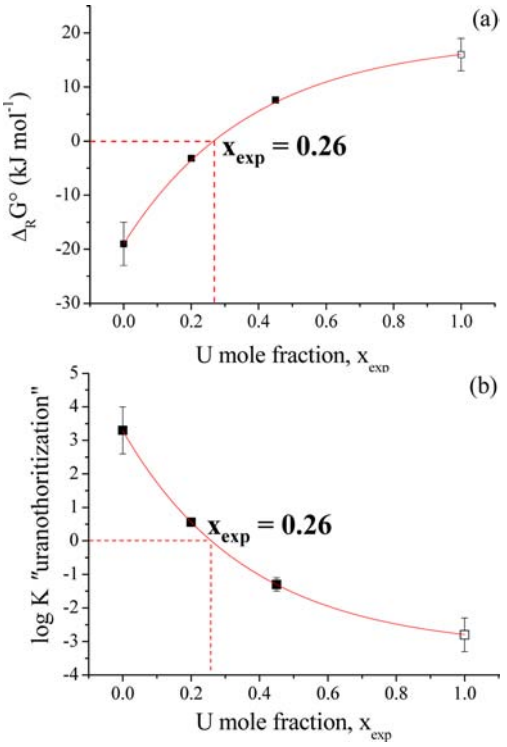

Figure 10. Variation of the calculated values of the standard Gibbs free energy of the "uranothoritization" reaction 15 at 298 K (a) and associated equilibrium constants (b) with the uranium mole fraction.

4. CONCLUSION

The ion activity products of uranothorite solid solutions were determined in a set of dissolution experiments conducted in 0.1 mol L^{-1} HCl under Ar atmosphere at several temperatures ranging from 298 to 346 K. For all experiments, the dissolution was congruent and a constant composition of the aqueous solution was reached after 50−200 days of dissolution depending on the experimental conditions. Constant distribution coefficients of U^{4+} and Th^{4+} with respect to the solid solution composition at stoichiometric saturation of the aqueous phase were obtained, indicating the preferential partitioning of U^{4+} toward the solid phase. Stoichiometric solubility products were also determined. This study reports the first experimental set of thermodynamic properties of intermediate members of the

dx.doi.org/10.1021/ic400272s | Inorg. Chem. 2013, 52, 6957−6968

uranothorite series. The stoichiometric solubility product of $Th_{1-x}U_xSiO_4$ solid solutions reached a maximum value for $x = 0.45 \pm 0.05$. In terms of the variation of the standard Gibbs free energy of dissolution, solid solutions dissolve more spontaneously than the end members. This behavior indicates that a metastable equilibrium might be reached during dissolution of uranothorite solid solutions. Owing to kinetic restrictions, coffinite (which is the most stable phase) did not precipitate, and the composition of the solid phase remained invariant.

From the distribution coefficients and the solubility product values of thorite ($\log {}^*K_{S,ThSiO_4} = -5.62 \pm 0.08$), the solubility product of coffinite was estimated as $\log {}^*K_{S,USiO_4} = -6.1 \pm 0.2$. This value is higher than that previously reported in the literature for coffinite. However, previous published values were not directly measured from solubility experiments but deduced from geochemical observations in uranium deposits where coffinite was observed, assuming that the silica concentration in groundwater was controlled by the solubility of coffinite. This assumption was already discussed in the literature, and chalcedony was identified as the phase that could potentially control the silica concentration in equilibrium with the uraninite−coffinite−SiO_2 system. Thus, the previously reported values could be underestimated. The study of the solubility of uranium-enriched uranothorites ($x > 0.5$) is now in progress to confirm these results.

The dissolution reaction of uranothorite solid solutions was found to be endothermic. The standard Gibbs free energy related to the formation of thorite, coffinite, and intermediate members of the series were evaluated. For the end members, the values obtained are in good agreement with previously reported data. The trend in the standard free energy of formation is a linear increase with the uranium mole fraction (Figure S1 of the Supporting Information). Considering the large uncertainties on the values obtained for the standard enthalpy of formation of $Th_{1-x}U_xSiO_4$ solid solutions, no significant trend was evidenced with the composition. Thus it was not possible to evaluate the stability of the uranothorite solid solutions and end members relative to their binary oxides at temperature higher than 298 K with good accuracy. Further investigations will be required to complete these data. However, the data presented in this paper at room temperature clearly show that uranothorite solid solutions with uranium mole fraction higher than 0.26, thus coffinite, are less stable than the mixture of the binary oxides, in agreement with qualitative evidence from petrographic studies of uranium ore deposits. These findings could thus improve the prediction of U(IV) mobility in the surrounding environment of underground SNF repository sites or at sites of groundwater contamination.

■ ASSOCIATED CONTENT

Supporting Information

Table S1 and Table S2 containing the thermodynamic data reported in the literature used in our calculations and variation of the $\Delta_f G^\circ$ of uranothorite solid solutions versus the uranium mole fraction (Figure S1). This material is available free of charge via the Internet at http://pubs.acs.org.

■ AUTHOR INFORMATION

Corresponding Author

*E-mail: stephanie.szenknect@cea.fr.

Notes

The authors declare no competing financial interest.

■ ACKNOWLEDGMENTS

Funding for this research was supported by the PACEN GUTEC (Geology of Uranium and Thorium: Extraction, Conversion) and by the NEEDS Ressources (mines, processes, economy), both programs of the CNRS. The authors are grateful to Dr. Dominique You (Department of Physical Chemistry, CEA) for very helpful comments regarding our results and to Johann Ravaux (Laboratory of Environmental Microscopy, ICSM) for the ESEM and X-EDS analyses.

■ REFERENCES

(1) Lebrun, P.; Cesbron, F.; Le Cleac'h, J. M.; Lebocey, J., *Minéraux uranifères. Uraninite et minéraux d'uranium dérivés ou associés*; Les eds. du Piat: France, 2009; p 176.

(2) Plant, J. A.; Simpson, P. R.; Smith, B.; Windley, B. F. *Rev. Mineral.* **1999**, *38*, 255−319.

(3) Voizard, P.; Mayer, S.; Ouzounian, G. *Icem 2007: Proceedings of the 11th International Conference on Environmental Remediation and Radioactive Waste Management, Pts A and B*; American Society of Mechanical Engineers: New York, 2009; pp 125−132

(4) Hogselius, P. *Energy Policy* **2009**, *37*, 254−263.

(5) Gaucher, É. C.; Blanc, P.; Bardot, F.; Braibant, G.; Buschaert, S.; Crouzet, C.; Gautier, A.; Girard, J.-P.; Jacquot, E.; Lassin, A.; Negrel, G.; Tournassat, C.; Vinsot, A.; Altmann, S. *C. R. Geosci.* **2006**, *338*, 917−930.

(6) Amme, M.; Wiss, T.; Thiele, H.; Boulet, P.; Lang, H. *J. Nucl. Mater.* **2005**, *341*, 209−223.

(7) Gaucher, E. C.; Tournassat, C.; Pearson, F. J.; Blanc, P.; Crouzet, C.; Lerouge, C.; Altmann, S. *Geochim. Cosmochim. Acta* **2009**, *73*, 6470−6487.

(8) Bruno, J.; Duro, L.; Grivé, M. *Chem. Geol.* **2002**, *190*, 371−393.

(9) Pomies, C.; Hamelin, B.; Lancelot, J.; Blomqvist, R. *Appl. Geochem.* **2004**, *19*, 273−288.

(10) Deditius, A. P.; Utsunomiya, S.; Ewing, R. C. *Chem. Geol.* **2008**, *251*, 33−49.

(11) Janeczek, J.; Ewing, R. C. *J. Nucl. Mater.* **1992**, *190*, 157−173.

(12) Grenthe, I.; Fuger, J.; Konings, R. J. M.; Lemire, R. J.; Muller, A. B.; Nguyen-Trung, C.; Wanner, H. *Chemical Thermodynamics of Uranium*; North Holland Elsevier Science Publishers B.V.: Amsterdan, The Netherlands, 1992; Vol. *1*, p 715.

(13) Guillaumont, R.; Fanghänel, T.; Fuger, J.; Grenthe, I.; Neck, V.; Palmer, D. A.; Rand, M. H., *Update on the Chemical Thermodynamics of Uranium, Neptunium, Plutonium, Americium and Technecium*; North Holland Elsevier Science Publishers B.V.: Amsterdam, The Netherlands, 2003; Vol. *5*, p 919.

(14) Langmuir, D. *Geochim. Cosmochim. Acta* **1978**, *42*, 547−569.

(15) Fuchs, L. H.; Hoekstra, H. R. *Am. Mineral.* **1959**, *44*, 1057−1063.

(16) Hemingway, B. S. Thermodynamic properties of selected uranium compounds and aqueous species at 298.15K and 1 bar and at higher temperatures. Preliminary models for the origine of coffinite deposits. US Geological Survey, 1982; p 89.

(17) Fleche, J. L. *Phys. Rev. B* **2002**, *65*, No. 245116.

(18) Mulak, J. *J. Solid State Chem.* **1977**, *21*, 117−126.

(19) Pointeau, V.; Deditius, A. P.; Miserque, F.; Renock, D.; Becker, U.; Zhang, J.; Clavier, N.; Dacheux, N.; Poinssot, C.; Ewing, R. C. *J. Nucl. Mater.* **2009**, *393*, 449−458.

(20) Reynolds, H.; Tardio, J.; Bhargava, S. Dissolution studies on synthetic coffinite. Presented at Chemeca 2011, Sydney, Australia, 2011.

(21) Costin, D. T.; Mesbah, A.; Clavier, N.; Szenknect, S.; Dacheux, N.; Poinssot, C.; Ravaux, J.; Brau, H. P. *Prog. Nucl. Energy* **2012**, *57*, 155−160.

(22) Costin, D. T.; Mesbah, A.; Clavier, N.; Dacheux, N.; Poinssot, C.; Szenknect, S.; Ravaux, J. *Inorg. Chem.* **2011**, *50*, 11117−11126.

(23) Fuchs, L. H.; Gebert, E. *Am. Mineral.* **1958**, *43*, 243−248.

(24) Finch, C. B.; Clark, G. W.; Harris, L. A. *Am. Mineral.* **1964**, *49*, 782−&.

(25) Burns, P. C. *Rev. Mineral.* **1999**, *38*, 23−90.

(26) Pointer, C. M.; Ashworth, J. R.; Ixer, R. A. *Mineral. Petrol.* **1988**, *39*, 21−37.
(27) Pointer, C. M.; Ashworth, J. R.; Ixer, R. A. *Mineral. Petrol.* **1988**, *38*, 245−262.
(28) Förster, H. J. *Lithos* **2006**, *88*, 35−55.
(29) Dacheux, N.; Brandel, V.; Genet, M. *New J. Chem.* **1995**, *19*, 1029−1036.
(30) Dacheux, N.; Brandel, V.; Genet, M.; Bak, K.; Berthier, C. *New J. Chem.* **1996**, *20*, 301−310.
(31) Finger, L. W.; Cox, D. E.; Jephcoat, A. P. *J. Appl. Crystallogr.* **1994**, *27*, 892−900.
(32) Rodríguez-Carvajal, J. *Phys. B* **1993**, *192*, 55−69.
(33) Taylor, M.; Ewing, R. C. *Trans., Am. Geophys. Union* **1975**, *56*, 1076−1076.
(34) Taylor, M.; Ewing, R. C. *Acta Crystallogr., Sect. B: Struct. Sci.* **1978**, *34*, 1074−1079.
(35) Flis, J.; Manecki, M.; Bajda, T. *Geochim. Cosmochim. Acta* **2011**, *75*, 1858−1868.
(36) Glynn, P. D.; Reardon, E. J. *Am. J. Sci.* **1990**, *290*, 164−201.
(37) Parkhurst, D. L.; Appelo, C. A. J. User's guide to PHREEQC (Version 2) - A computer program for speciation, batch reaction, one-dimensional transport, and inverse geochemical calculations. U.S.G.S. Water-Resources Investigations Report 99-4259; 1999.
(38) Johnson, J. W.; Oelkers, E. H.; Helgeson, H. C. *Comput. Geosci.* **1992**, *18*, 899−947.
(39) Oelkers, E. H.; Bénézeth, P.; Pokrovski, G. S., Thermodynamic Databases for Water-Rock Interaction. In *Thermodynamics and Kinetics of Water-Rock Interaction*; Oelkers, E. H., Schott, J., Eds.; Reviews in Mineralogy & Geochemistry; Mineralogical Society of America: St. Louis, MO, 2009; Vol. *70*, pp 1−46.
(40) Appelo, C. A. J.; Postma, D. *Geochemistry, Groundwater and Pollution*. A.A. Balkema: Rotterdam, Netherlands: 1996; p 536.
(41) Glynn, P. D.; Reardon, E. J.; Plummer, L. N.; Busenberg, E. *Geochim. Cosmochim. Acta* **1990**, *54*, 267−282.
(42) Lippmann, F. *N. Jahrb. Mineral. Abh.* **1977**, *130*, 243−263.
(43) Lippmann, F. *N. Jahrb. Mineral. Abh.* **1980**, *139*, 1−25.
(44) Thorstenson, D. C.; Plummer, L. N. *Am. J. Sci.* **1977**, *277*, 1203−1223.
(45) Prieto, M. Thermodynamics of Solid Solution-Aqueous Solution Systems. In *Thermodynamics and Kinetics of Water-Rock Interaction*; Oelkers, E. H.; Schott, J., Eds.; Mineralogical Society of America: St. Louis, MO, 2009; Vol. *70*, pp 47−85.
(46) Bruno, J.; Bosbach, D.; Kulik, D.; Navrotsky, A., *Chemical Thermodynamics of Solid Solutions of Interest in Nuclear Waste Management*; North holland Elsevier Science Publishers B.V.: Amsterdam, The Netherlands: 2007; Vol. *10*, p 267.
(47) Dandurand, J. L.; Schott, J. *Bull. Minéral.* **1980**, *103*, 307−316.
(48) Tesoriero, A. J.; Pankow, J. F. *Geochim. Cosmochim. Acta* **1996**, *60*, 1053−1063.
(49) Brookins, D. G. *Am. Assoc. Pet. Geol., AAPG Bull.* **1975**, *59*, 905−905.
(50) Langmuir, D. *Aqueous Environmental Geochemistry*; Prentice Hall: Upper Saddle River, NJ, 1997.
(51) Schuiling, R. D.; Vergouwen, L.; Vanderrijst, H. *Am. Mineral.* **1976**, *61*, 166−168.
(52) Mazeina, L.; Ushakov, S. V.; Navrotsky, A.; Boatner, L. A. *Geochim. Cosmochim. Acta* **2005**, *69*, 4675−4683.
(53) Rand, M.; Fuger, J.; Grenthe, I.; Neck, V.; Rai, D. *Chemical Thermodynamics of Thorium*; OECD Publications: Paris, France, 2009; Vol. *11*, p 900.
(54) Navrotsky, A. *Rev. Mineral.* **1987**, *17*, 35−69.
(55) Mumpton, F. A.; Roy, R. *Geochim. Cosmochim. Acta* **1961**, *21*, 217−238.